Arabidopsis calmodulin-like protein CML36 is a calcium (Ca^{2+}) sensor that interacts with the plasma membrane Ca^{2+}-ATPase isoform ACA8 and stimulates its activity

Received for publication, March 23, 2017, and in revised form, July 7, 2017 Published, Papers in Press, July 18, 2017, DOI 10.1074/jbc.M117.787796

Alessandra Astegno[‡1], Maria Cristina Bonza[§], Rosario Vallone[‡], Valentina La Verde[‡], Mariapina D'Onofrio[‡], Laura Luoni[§], Barbara Molesini[‡], and Paola Dominici[‡]

From the [‡]Department of Biotechnology, University of Verona, Strada Le Grazie 15, 37134 Verona, Italy and the [§]Department of Biosciences, University of Milano, Via Celoria 26, 20133 Milano, Italy

Edited by Joseph Jez

Calmodulin-like (CML) proteins are major EF-hand–containing, calcium (Ca^{2+})–binding proteins with crucial roles in plant development and in coordinating plant stress tolerance. Given their abundance in plants, the properties of Ca^{2+} sensors and identification of novel target proteins of CMLs deserve special attention. To this end, we recombinantly produced and biochemically characterized CML36 from *Arabidopsis thaliana*. We analyzed Ca^{2+} and Mg^{2+} binding to the individual EF-hands, observed metal-induced conformational changes, and identified a physiologically relevant target. CML36 possesses two high-affinity Ca^{2+}/Mg^{2+} mixed binding sites and two low-affinity Ca^{2+}-specific sites. Binding of Ca^{2+} induced an increase in the α-helical content and a conformational change that lead to the exposure of hydrophobic regions responsible for target protein recognition. Cation binding, either Ca^{2+} or Mg^{2+}, stabilized the secondary and tertiary structures of CML36, guiding a large structural transition from a molten globule apo-state to a compact holoconformation. Importantly, through *in vitro* binding and activity assays, we showed that CML36 interacts directly with the regulative N terminus of the *Arabidopsis* plasma membrane Ca^{2+}-ATPase isoform 8 (ACA8) and that this interaction stimulates ACA8 activity. Gene expression analysis revealed that *CML36* and *ACA8* are co-expressed mainly in inflorescences. Collectively, our results support a role for CML36 as a Ca^{2+} sensor that binds to and modulates ACA8, uncovering a possible involvement of the CML protein family in the modulation of plant-autoinhibited Ca^{2+} pumps.

Calcium (Ca^{2+}) is a crucial second messenger in plants, where it couples the perception of endogenous and environmental signals to plant responses (1–4). Ca^{2+} signals are transmitted by stimulus-specific cytosolic Ca^{2+} elevations that result from the concerted action of both Ca^{2+} influx (channels) and Ca^{2+} efflux (pumps and carriers) systems, which temporally shape and spatially define Ca^{2+} dynamics, commonly referred to as the "Ca^{2+} signature" (3–6). These signatures are believed to encode information from primary stimuli and, therefore, to contribute to the stimulus specificity of the biological response. Nonetheless, another layer of specificity in Ca^{2+} signaling is achieved via the function of Ca^{2+} sensors, which detect alterations in intracellular free Ca^{2+} concentration decoding specific Ca^{2+} signatures into downstream physiological responses (7). Most Ca^{2+} sensors harbor the EF-hand motif, a helix-loop-helix structure binding one Ca^{2+} ion. The EF-hand binds Ca^{2+} through a pentagonal bipyramidal arrangement, and the chelating residues are notated either based on their linear positions (1, 3, 5, 7, 9, and 12) or on their tertiary coordination geometry (X, Y, Z, −Y, −X, and −Z) (8). In the canonical EF-hand, positions 1 (X), 3 (Y), 5 (Z), and 12 (−Z) are side-chain oxygen ligands, 7 (−Y) is a backbone carbonyl ligand, and 9 (−X) is a water ligand hydrogen-bonded to one loop residue (8). Ca^{2+} binding modifies the conformation of EF-hand proteins resulting in changes in enzymatic activity of the Ca^{2+} sensor itself or allowing it to interact with and alter the target protein activity (9). Besides calmodulin (CaM),[2] which has been well-conserved during evolution, plants contain a unique family (50 members in the model plant *Arabidopsis thaliana*) of CaM-like proteins (CMLs) that greatly differ from canonical CaMs in sequence (they share at least 16% overall amino acid identity with CaM2 of *Arabidopsis*), length (some CMLs possess N- or C-terminal extensions), and number of EF-hands (from 1 to 6) (10–12). Functional analyses of various plant CMLs have provided clear indications for the key roles of these proteins in plant development and abiotic and biotic stress responses, as overviewed in several recent reviews (12–15). Altogether, these studies do not support a functional redundancy hypothesis for CMLs, which could be key positive and/or negative regulator components in the coordination of plant responses to different environmental stimuli (15). However, to date only a few of these proteins have been clearly shown to function as Ca^{2+} sensors by describing their Ca^{2+}-binding (*e.g.* dissociation constants, stoichiometry, ligand specificity) and structural properties and by

This study was supported in part by Grant FUR2014 from the University of Verona (to A. A. and P. D.). The authors declare that they have no conflicts of interest with the contents of this article.

This article contains supplemental Figs. S1 and S2 and "Methods."

[1] To whom correspondence should be addressed: Dept. of Biotechnology, University of Verona, Strada Le Grazie 15, Verona (VR), Italy. Tel.: 39-045-8027955; Fax: 39-045-8027929; E-mail: alessandra.astegno@univr.it.

[2] The abbreviations used are: CaM, calmodulin; CML, CaM-like protein; ACA8, Ca^{2+}-ATPase isoform 8; CML36 f.l., full-length CML36; PM, plasma membrane; ANS, 1-anilino-8-naphthalene sulfonate; SEC, size-exclusion chromatography; ITC, isothermal titration calorimetry; HSQC, heteronuclear single-quantum coherence; DSS, 2,2-dimethyl-2-silapentanesulfonic acid; Tricine, *N*-[2-hydroxy-1,1-bis(hydroxymethyl)ethyl]glycine.

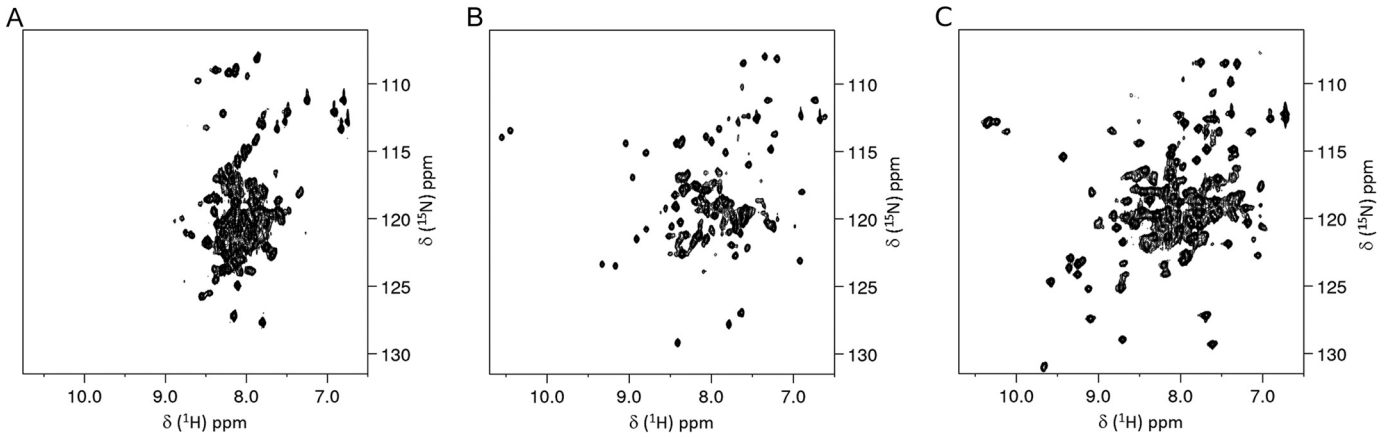

Figure 1. Two-dimensional ^{1}H-^{15}N HSQC NMR spectra of ^{15}N-CML36-C. The spectra were recorded at 600 MHz and 25 °C in the presence of 5 mM EGTA (*A*), 5 mM $MgCl_2$ (*B*), and 5 mM $CaCl_2$ (*C*). All samples were at a protein concentration of 500 μM in 20 mM Tris-HCl, 1 mM DTT, pH 7.5.

identifying their biological targets. Thus, a detailed characterization of CMLs at the biochemical and structural levels combined with the identification of distinct downstream targets is essential in determining the high level of specificity that allows the plant cell to transduce diverse stimuli into proper physiological responses.

In the present study, we characterized CML36 from *A. thaliana.* In particular, using different complementary biophysical and biochemical methods, we analyzed whether CML36 possesses the structural and binding properties of Ca^{2+} sensor proteins. We found that CML36 behaves as a Ca^{2+} sensor, in that it experiences Ca^{2+}-dependent changes in secondary and tertiary structure and in the exposure of hydrophobic regions. Moreover, we identified a biological target, providing evidence that CML36 interacts directly with *Arabidopsis* Ca^{2+}-ATPase isoform 8 (ACA8), a type IIB Ca^{2+} pump localized at the plasma membrane (PM) that contributes to the overall Ca^{2+} homoeostasis and to the control of intracellular Ca^{2+} signaling by actively extruding Ca^{2+} from the cytosol into the apoplast (16–18). We identified the specific CML36-binding site at the N terminus of ACA8 and demonstrated that the interaction between ACA8 and CML36 promotes the pump Ca^{2+}-dependent hydrolytic activity *in vitro*. Collectively, our findings allowed us to classify CML36 as a Ca^{2+} sensor, uncovering a possible involvement of CML36 in the modulation of the plant autoinhibited Ca^{2+} pump.

Results

CML36 is a Ca^{2+} sensor

Recombinant production of full-length CML36 (CML36 f.l.) resulted in a highly unstable protein (with a high propensity to aggregate and precipitate) at the concentrations required for efficient protein-based biophysical and structural analyses. CML36 contains an extended N-terminal region (residues 1–60) and a Ca^{2+}-binding region (residues 61–209) with four EF-hand motifs. The extended N-terminal region was found to be remarkably intrinsically disordered using the GeneSilico MetaDisorder Service (19), and therefore a truncated variant of CML36 was created by deleting the first 60 residues. The resulting mutant (residues 61–209, named CML36-C) was very stable even at high concentrations and was therefore used for all biophysical and structural analyses.

Typical features of Ca^{2+} sensors include Ca^{2+}-induced conformational changes that often expose hydrophobic surfaces necessary for target recognition. Thus, we examined Ca^{2+}-dependent conformational changes and surface hydrophobicity of recombinant CML36-C by using an array of biophysical and structural techniques such as nuclear magnetic resonance (NMR), circular dichroism (CD), 1-anilino-8-naphthalene sulfonate (ANS) fluorescence spectroscopy, and size-exclusion chromatography (SEC). Moreover, because of the high concentration of free Mg^{2+} in plant cells (0.5–2 mM) (20, 21) we also analyzed the behavior of CML36-C upon the addition of Mg^{2+}, to determine the specificity of CML36 in discriminating cytosolic Ca^{2+} signals against a $\sim 10^2$–10^4-fold excess of the chemically similar divalent cation Mg^{2+}. Mg^{2+} binding to EF-hands is physiologically important; distinct roles have been proposed for the binding of this ion (8, 22), such as a structural role, by conferring structural stability to an otherwise poorly defined molten globule apo-state, or roles in the Ca^{2+}-dependent regulation of cellular processes by modulating the affinity of EF-hands for Ca^{2+}.

NMR spectroscopy was used to investigate the structural rearrangements of CML36-C upon the addition of metal ions. The signals in a two-dimensional ^{1}H-^{15}N heteronuclear single-quantum coherence (HSQC) NMR spectrum belong to the HN groups of the protein. The frequency of HN signals (chemical shift) correlates with the chemical environment of the observed nuclei and is influenced by both local and global structure.

The ^{1}H-^{15}N HSQC spectrum of apoCML36-C is characterized by the presence of fewer peaks than expected, severe line broadening, and poor chemical shift dispersion, especially in the proton dimension (Fig. 1*A*). These spectral features suggest that apoCML36-C undergoes conformational fluctuations typical of a molten globule state, similar to other EF-hand proteins in their apoforms (23–25). A change in the HSQC spectrum of CML36-C was observed upon the addition of a saturating concentration of Mg^{2+} (Fig. 1*B*). The spectrum is characterized by more uniform peak intensities and an increased chemical shift dispersion, indicating that Mg^{2+}-bound CML36-C adopts a

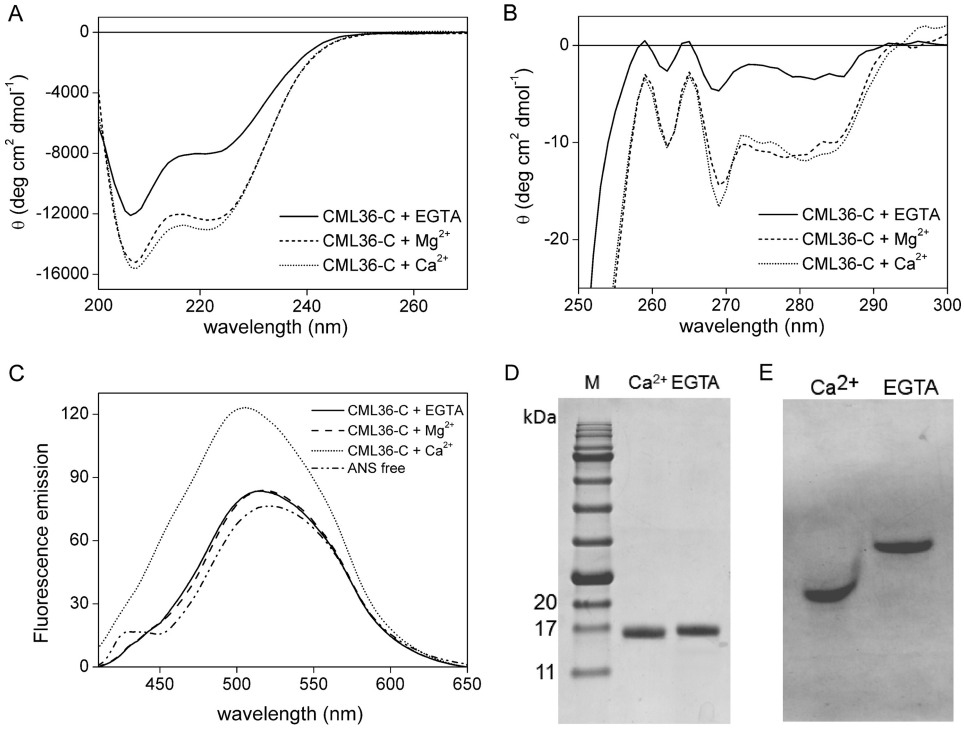

Figure 2. Ca^{2+} sensor properties of CML36-C. *A* and *B*, far-UV CD spectra of 10 μM CML36-C (*A*) and near-UV CD spectra of 90 μM CML36-C (*B*) in the presence of 5 mM EGTA (*solid line*), 5 mM $MgCl_2$ (*dashed line*), and 5 mM $CaCl_2$ (*dotted line*). *C*, ANS-fluorescence of CML36-C in the presence of 5 mM EGTA (*solid line*), 5 mM $MgCl_2$ (*dashed line*), and 5 mM $CaCl_2$ (*dotted line*). The spectrum of ANS alone (*dash-dotted line*) is also shown. *D*, SDS-PAGE mobility shift of CML36-C in the presence of 5 mM $CaCl_2$ or 5 mM EGTA. *Lane M* is a molecular mass marker. *E*, native PAGE mobility shift of CML36-C in the presence of 5 mM $CaCl_2$ or 5 mM EGTA.

more stable tertiary structure compared with the apoprotein. However, the number of peaks in the Mg^{2+}-bound form remained much lower than expected considering the non-proline residues in the amino acid sequence of CML36-C (150 residues), and many peaks in the central area of the HSQC spectrum still appeared rather broad, meaning that some portions of the Mg^{2+}-bound protein may not be structured or may still possess a high degree of flexibility. Remarkably, the addition of saturating Ca^{2+} concentrations to the apoCML36-C resulted in a more dramatic change in the CML36-C HSQC spectrum, where ~120 peaks with good chemical shift dispersion became visible (Fig. 1*C*), indicating that the addition of Ca^{2+} promotes a global structural rearrangement throughout the protein. By comparing the position of the peaks in the two metal-bound forms, it was evident that Ca^{2+} induced conformational changes in CML36-C distinct and separate from those induced by Mg^{2+}, which is in line with a putative Ca^{2+} sensor function of the protein.

The far- and near-UV CD analyses were consistent with the interpretation of the apoCML36-C as a molten globule state, as in apoCML36-C the secondary structure is conserved to a large extent, whereas the tertiary structure is highly fluctuating. *Panels A* and *B* of Fig. 2 show the far- and near-UV regions of the CD spectra of apoCML36-C and Ca^{2+}- or Mg^{2+}-bound CML36-C, respectively. As evident in Fig. 2*A*, the far-UV CD spectra for the apoform and both holoforms of CML36-C show two negative bands with minima at 208 and 222 nm, characteristic of proteins with a high α-helical content. However, the reduced $\theta_{222/208}$ ratio observed in apoCML36-C (0.67 for apoCML36-C *versus* 0.83 and 0.82 for Ca^{2+}-CML36-C and Mg^{2+}-CML36-C, respectively) suggests the presence of some regions of high flexibility or random coil structures.

Despite the absence of Trp residues, CML36-C has two Tyr and eight Phe residues, and the corresponding bands are well-resolved in the near-UV CD spectra (Fig. 2*B*). Signals in the 275–290-nm range can be associated with the microenvironment of Tyr residues, whereas the bands observed in the 250–270-nm region, with minima at 262 and 268 nm, are ascribable to Phe residues. The switch of CML36-C from the holo- to the apoform produces considerable changes in this part of the CD spectrum (Fig. 2*B*), suggesting a partial collapse of the tertiary structure.

A common feature of Ca^{2+} sensors is the increase in surface-exposed hydrophobicity upon Ca^{2+} binding, which we investigated by the use of the fluorescent probe ANS. This dye is a hydrophobic compound that shows a blue-shift in the maximum emission and a considerable increase in fluorescence upon binding to hydrophobic regions of proteins. In the presence of apoCML36-C, we detected a ~7-nm blue-shift and a modest increase in the emission of ANS in comparison with ANS alone (Fig. 2*C*), suggesting that apoCML36-C possesses exposed hydrophobic portions. The addition of Mg^{2+} did not cause further changes to the spectrum, whereas upon the addition of Ca^{2+} a further blue-shift (~12 nm) and a 1.6-fold increase in fluorescence emission was observed, indicating that CML36-C undergoes a Ca^{2+}-dependent exposure of hydrophobic surfaces.

Analytical SEC, together with pulsed-field gradient diffusion NMR studies, was conducted to examine the hydrodynamic radius (R_h) of CML36-C in the apo-state and the Mg^{2+}-bound

and Ca^{2+}-bound states (Table 1). Notably, in all of these states, the obtained R_h resulted in an apparent molecular mass overestimation, which has been observed in various Ca^{2+} sensor proteins (26–28) and is related to their extended conformation. Moreover, the binding of Ca^{2+}, and to a less extent of Mg^{2+}, to CML36-C determined a decrease in R_h, as found elsewhere for CaMs (26, 27, 29).

Altogether, these structural studies strongly suggest that CML36-C functions as Ca^{2+} sensor, indicating that apoCML36-C is in a dynamic molten globule form that undergoes a large conformational change upon binding Ca^{2+}. Moreover, CML36-C displays a higher electrophoretic mobility in the presence of Ca^{2+} both in denaturing and native conditions (Fig. 2, *D* and *E*), which is a well-documented phenomenon for CaM proteins (29–32).

Table 1

Determination of hydrodynamic radius of apo- and holoCML36-C by pulsed-field gradient diffusion NMR analysis and SEC

The mean values ± S.E. from triplicate experiments are presented. *D*, diffusion coefficient; R_h, hydrodynamic radius.

	Pulsed-field gradient diffusion NMR		
	D	R_h	SEC R_h
	10^{-10} m^2 s^{-1}	Å	Å
CML36-C + EGTA	0.99 ± 0.02	25.6 ± 1.2	29.5 ± 0.02
CML36-C + Mg^{2+}	1.08 ± 0.08	21.3 ± 2.3	25.0 ± 0.03
CML36-C + Ca^{2+}	1.19 ± 0.02	20.9 ± 0.7	23.2 ± 0.2

CML36 contains four Ca^{2+}-binding sites

Isothermal titration calorimetry (ITC) was used to monitor Ca^{2+} and Mg^{2+} binding to CML36-C, which allows the determination of accurate values of apparent dissociation constants (K_d) for multiple binding sites and related changes in enthalpy (ΔH). Representative ITC isotherms are shown in Fig. 3, and the thermodynamic binding parameters obtained are listed in Table 2. Titration of $CaCl_2$ into apoCML36-C at physiological salt concentrations (Fig. 3*A*, *black line*) produced a multiphasic binding isotherm with an initial exothermic phase followed by an endothermic phase. The data best fit a four-site sequential binding model that reflected the presence of two classes of binding sites (Table 2): the first class comprises two high-affin-

Table 2

Thermodynamics of Ca^{2+} binding to CML36-C in the absence and presence of Mg^{2+}

The mean values ± S.E. from triplicate experiments using at least two different CML36-C preparations are presented.

	No Mg^{2+}		+5 mM Mg^{2+}	
	K_a	ΔH	K_a	ΔH
	M^{-1}	kcal mol^{-1}	M^{-1}	kcal mol^{-1}
Site 1	1.1*E*7 ± 0.6*E*7	−11.9 ± 0.5	3.5*E*6 ± 0.5*E*6	−6.6 ± 0.1
Site 2	8.2*E*6 ± 0.9*E*6	−9.6 ± 0.6	1.8*E*6 ± 0.3*E*6	−6.1 ± 0.2
Site 3	9.6*E*3 ± 0.8*E*3	3.6 ± 0.4	8.7*E*3 ± 1.1*E*3	2.8 ± 0.1
Site 4	2.9*E*3 ± 0.2*E*3	2.2 ± 0.1	3.2*E*3 ± 0.4*E*3	2.0 ± 0.3

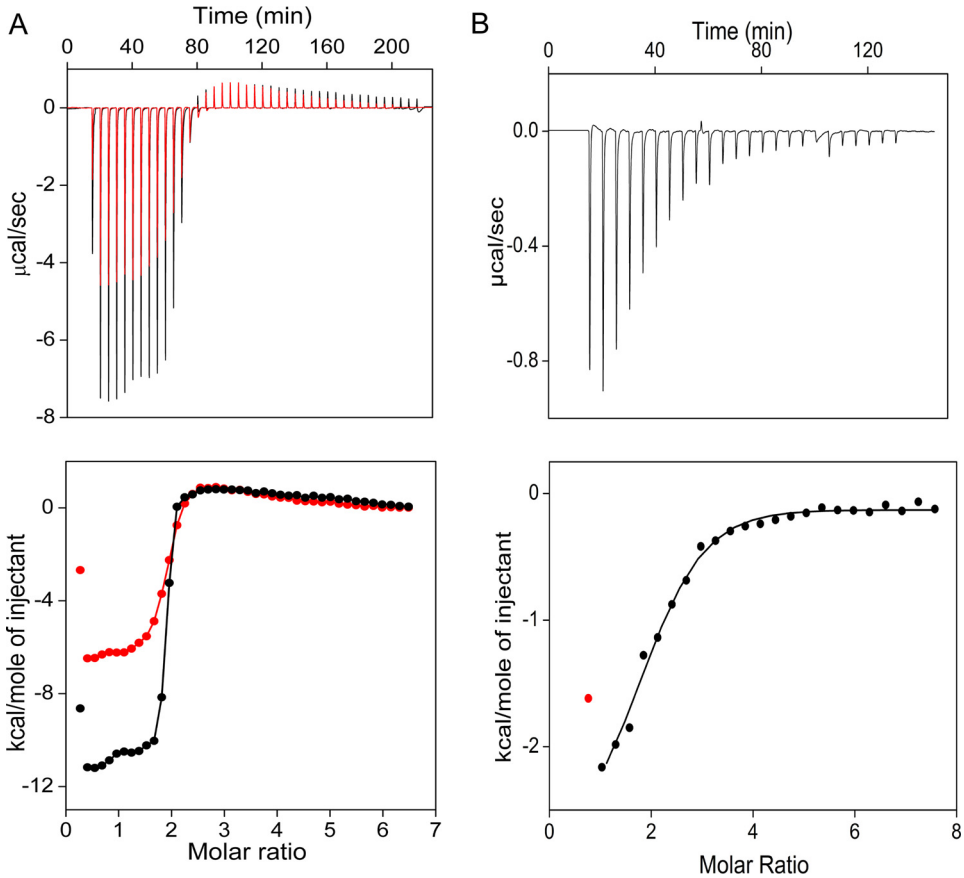

Figure 3. ITC analysis of Ca^{2+} binding to apoCML36-C and Mg^{2+}-bound CML36-C (*A*) and Mg^{2+} binding to apoCML36-C (*B*). Representative data curves are shown of the calorimetric titrations of 4 mM $CaCl_2$ into apoCML36-C (*A*, *black lines*) and Mg^{2+}-bound CML36-C (*A*, *red lines*) and of calorimetric titrations of 5 mM $MgCl_2$ into apoCML36-C (*B*). The *upper panels* represent raw traces minus baseline of the calorimetric titrations, and the *lower panels* show the corresponding integrated binding isotherms. Under all applied conditions, the reference baseline data obtained by Mg^{2+} and Ca^{2+} ions titrated into buffer only showed very weak dilution heat produced during the reaction (data not shown). The ligand dilution blank experiments were then subtracted from the binding isotherm obtained in the presence of protein.

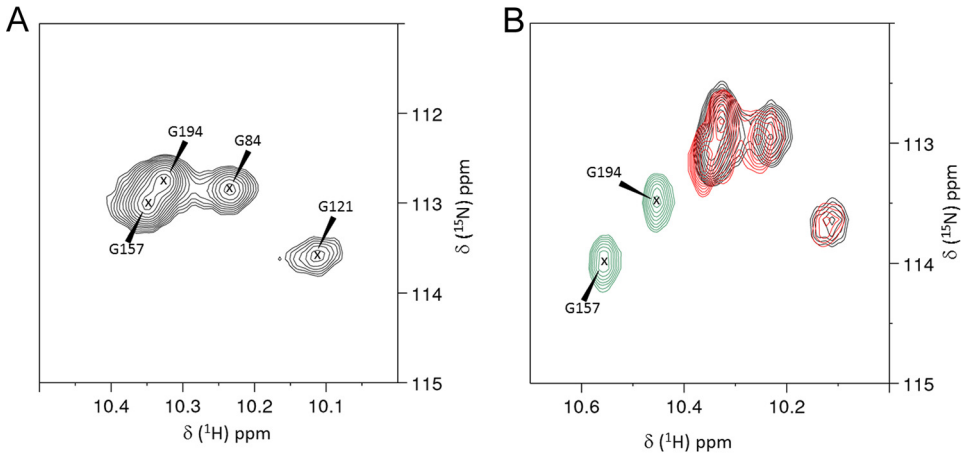

Figure 4. Zoom view of the ^{1}H-^{15}N HSQC NMR spectra of the glycine downfield peaks of ^{15}N-CML36-C. *A*, portion of the HSQC spectrum of CML36-C in complex with Ca^{2+} ion. The assignment of the glycines of the EF-hands is indicated by the *position number* of the residue. *B*, superimposition of HSQC spectra recorded on ^{15}N-CML36-C after the addition of Mg^{2+} (*green*), Ca^{2+} (*black*), and Ca^{2+} into Mg^{2+}-saturated protein (*red*). The spectra were recorded at 600 MHz and 25 °C. All samples were at a protein concentration of 500 μM in 20 mM Tris-HCl, 1 mM DTT, pH 7.5.

ity sites (K_{d1} = 91 ± 17 nM and K_{d2} = 122 ± 13 nM, respectively) with a heat release between −12 and −10 kcal/mol of $CaCl_2$; and the second class likely represents the binding of two Ca^{2+} ions with lower affinity (K_{d3} = 104 ± 9 μM and K_{d4} = 345 ± 24 μM) with $\Delta H \sim 3$ kcal/mol of $CaCl_2$. The Ca^{2+} titration was also performed in the presence of 5 mM Mg^{2+} (Fig. 3*A*, *red line*, and Table 2). Mg^{2+} did not greatly affect the affinity constants associated with Ca^{2+} binding to sites 3 and 4 of CML36-C, indicating no binding of Mg^{2+} to these sites, whereas the K_d values of sites 1 and 2 were shifted to lower affinity. Moreover, Mg^{2+} had an effect on the ΔH of sites 1 and 2, as the process was less exothermic than that without Mg^{2+}. This behavior, likely suggesting that in the presence of Mg^{2+} these two sites could be formed and structurally stable, prompted us to quantitate the direct binding of Mg^{2+} to CML36-C. Titration of $MgCl_2$ into apoCML36-C resulted in an exothermic binding isotherm (Fig. 3*B*), giving the best fit with the binding of two Mg^{2+} ions to protein with a K_a value of 9.2*E*3 ± 0.7*E*3 M^{-1} (which corresponds to a K_d value of 109 ± 8 μM), an enthalpy ΔH of −3.9 ± 0.7 kcal mol^{-1}.

The stoichiometry of Ca^{2+} and Mg^{2+} binding was further confirmed by analysis of the ^{1}H-^{15}N HSQC NMR spectra of CML36-C. Downfield-shifted NMR peaks at ~10.5 ppm are typical of conserved glycines at position 6 of the EF-hands occupied by divalent metals (25, 33, 34). In Ca^{2+}-saturated CML36-C, the presence of four downfield-shifted peaks corresponding to Gly-84 (EF-1), Gly-121 (EF-2), Gly-157 (EF-3), and Gly-194 (EF-4) confirms that Ca^{2+} is bound to the four EF-hands, as seen by ITC analysis (Fig. 4*A*). The addition of saturating amounts of Mg^{2+} to apoCML36-C caused the appearance of two downfield-shifted NMR peaks, assigned to Gly-157 and Gly-194 (Fig. 4*B*, *green*), indicating that Mg^{2+} is bound to EF-3 and EF-4. Notably, the addition of Ca^{2+} to Mg^{2+}-bound CML36-C caused the two downfield peaks at 10.55 ppm (Gly-157) and 10.45 ppm (Gly-194) to disappear and the appearance of the four glycine peaks in the position typical of the Ca^{2+}-bound protein (Fig. 4*B*, *red*), suggesting that the Ca^{2+} ion could displace Mg^{2+} from EF-3 and EF-4.

CML36 interacts with ACA8 and stimulates its Ca^{2+}-dependent hydrolytic activity

To fully understand the roles of Ca^{2+} sensors, the identification of physiologically relevant targets is essential. A bioinformatics search for possible interactors of CML36 using string database (http://string-db.org/), which gives extensive coverage and ease of access to both experimental and predicted interaction information (35), found several promising candidates with various confidence scores. Among all of the putative predicted interactors, we decided to focus on the PM-localized type IIB Ca^{2+}-ATPase isoform ACA8 because: (i) it is a prominent *in vivo* regulator of cellular Ca^{2+} dynamics (18); (ii) *CML36* transcript has been found to be altered in an *Arabidopsis* double mutant lacking both ACA8 and ACA10, another PM-localized Ca^{2+}-ATPase isoform (36); and (iii) in a phosphoproteomic study, CML36 has been shown to be associated with the PM fraction, which might facilitate the interaction with ACA8 *in vivo* (37). ACA8 possesses an extended cytosolic N-terminal regulatory domain with autoinhibitory function (16, 38–40). The best-known regulator of ACA8 is CaM. CaM binding to the N terminus induces a conformational change that suppresses autoinhibition, thus determining the activation of the pump. The N terminus is the target of modulation not only by CaM but also by other regulators of the pump, such as acidic phospholipids, which counteract its autoinhibitory action (41). In addition, the phosphoregulation of N-terminal serine residues by influencing autoinhibition (42) is associated with alterations of the intracellular Ca^{2+} dynamics in response to mechanical wounding (18). As a first step toward experimental validation of the putative interaction between CML36 and ACA8, we performed an *in vitro* overlay assay by spotting increasing amounts of recombinant CML36-C onto nitrocellulose and testing its ability to bind purified ACA8. We used bovine CaM and lysozyme as the positive and negative controls, respectively. Moreover, we tested another member of the *Arabidopsis* CML family, CML14 (43), which was not predicted to interact with ACA8. Specific interaction of ACA8 with CML36-C and CaM was evident (Fig. 5*A*). A signal of interaction with CML14 was

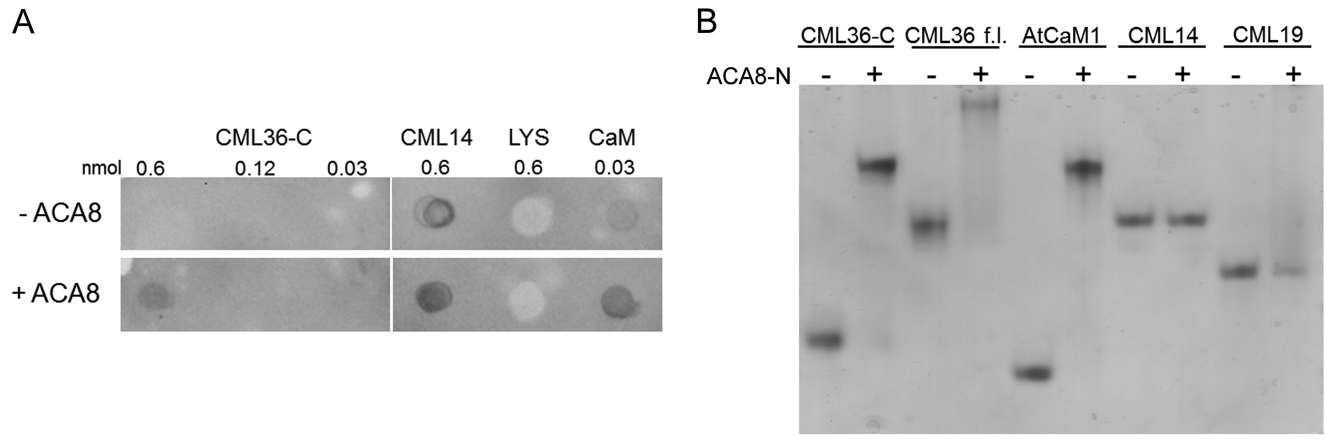

Figure 5. ACA8/CML36-binding assays. *A*, overlay assay. Two μl of native Ca^{2+}-bound CML36-C corresponding to 0.6, 0.12, or 0.03 nmol was spotted onto 0.2 μm nitrocellulose. After a cross-linking step, the overlay assay was performed by incubating the membrane without (*upper panel*) or with (*lower panel*) 1.5 μM purified ACA8 in the presence of 200 μM $CaCl_2$ and 2 mM $MgSO_4$ as described under "Experimental procedures." Detection was performed using an anti-ACA8 antiserum. As a control, 0.6 nmol of CML14, 0.6 nmol of lysozyme, and 0.03 nmol of bovine testes CaM were used. Data are from one experiment representative of three that gave similar results. *B*, native PAGE analysis of CML36-C, CML36 f.l., AtCaM1, CML14, and CML19 in the absence and presence of ACA8-N in 100 mM Tris-HCl, 5 mM $CaCl_2$, and 4 M urea, pH 7.5.

visible, but a similar signal intensity was also observed when the nitrocellulose was incubated in the absence of ACA8 (Fig. 5*A*), strongly suggesting nonspecific binding of the anti-ACA8 antibody to CML14.

The specificity of the ACA8-CML36 interaction was also supported by native PAGE analysis (Fig. 5*B*). We produced in recombinant form the N-terminal portion of ACA8 corresponding to the regulatory domain (residues 1–116, named ACA8-N), and we checked the interaction between ACA8-N and both CML36-C and CML36 f.l. Recombinant *Arabidopsis* CaM1 (AtCaM1) was used as positive control and two other CMLs, *i.e.* CML14 and CML19, as negative controls. When ACA8-N and CML36 (both CML36-C and CML36 f.l. variants) were mixed in the presence of Ca^{2+}, an additional band appeared on the native gel, likely representing the CML36-ACA8-N complex. An extra band was also visible for the AtCaM1-ACA8-N complex, whereas it was missing in the CML19- and CML14-containing samples, indicating the inability of these two CML isoforms to form a complex with ACA8-N. These results clearly confirmed the ability of CML36 to interact with ACA8 and localized the CML-binding domain to a region in the N terminus of the enzyme.

To elucidate the relevance of the CML36-ACA8 interaction, we subsequently examined its effect on ACA8 activity by measuring, in the presence of increasing concentrations of Ca^{2+}-bound CML36, the hydrolytic activity of ACA8 overexpressed in the yeast triple mutant K616, which is defective in high-affinity endogenous Ca^{2+} pumps (38, 40, 44). Fig. 6*A* shows that the Ca^{2+}-dependent hydrolytic activity of ACA8 was significantly stimulated by CML36-C in a concentration-dependent manner. The concentration of CML36-C giving half-maximal stimulation of ACA8 activity ($K_{0.5}$) was 534 $\pm$ 42 nM. The activation of the Ca^{2+}-ATPase was specific for CML36-C, as the addition of similar concentrations of two other CMLs, CML14 (Fig. 6*A*) and CML19 (data not shown), was completely ineffective. To exclude the possibility that the CML36-C might lack portions with a potential regulatory role, we also performed the same experiment with CML36 f.l. The results showed that the ACA8 activation curve in the presence of increasing concentrations of CML36 f.l. was comparable to that obtained using the truncated variant, CML36-C (supplemental Fig. S1).

The effect of CML36 on ACA8 activity was further evaluated in the presence of saturating CaM. As expected, the enzymatic activity of ACA8 was increased by CaM (42, 45). The addition of increasing concentrations of CML36-C did not influence CaM-stimulated enzymatic activity (Fig. 6*A*), revealing that the two effects were not additive. Thus, in accordance with the native PAGE results, we determined that CML36 and CaM interact within the N-terminal region of ACA8. Consistently, the response to CML36-C of the two N-terminal truncated mutants of ACA8 (Δ74ACA8 and Δ109ACA8, from which the high-affinity and both the high- and low-affinity CaM-binding sites, respectively, have been deleted (38, 46)) was completely suppressed (Fig. 6*B*).

Because the above-described experiments were carried out on yeast microsomes overexpressing ACA8, to further corroborate our results we evaluated the response to CML36-C of ACA8 following a one-step purification on CaM-Sepharose. Fig. 6*C* shows that, under the experimental conditions used, the ACA8 activation curve resembled that obtained using the microsomal fraction, with an estimated $K_{0.5}$ value of 797 $\pm$ 168 nM. Moreover, we confirmed the specificity of the CML36-C effect, as no ACA8 activation was detected in the presence of the other two CMLs, *i.e.* CML14 (Fig. 6*C*) and CML19 (data not shown). As shown in Fig. 6*A*, ACA8 was not further stimulated by CML36-C when activated by saturating CaM. We then tested the ability of 4.2 μM CML36-C to stimulate the ATPase activity in the presence of increasing, but subsaturating, CaM concentrations. The results, reported in Fig. 6*D*, indicate an additive effect of CML36-C and CaM that was evident only in the presence of low CaM concentrations. This finding is in accordance with competition between the two activating proteins.

Expression pattern analysis of CML36 in different Arabidopsis organs

Quantitative RT-PCR performed on adult *Arabidopsis* plants indicated that the *CML36* gene is ubiquitously expressed but is

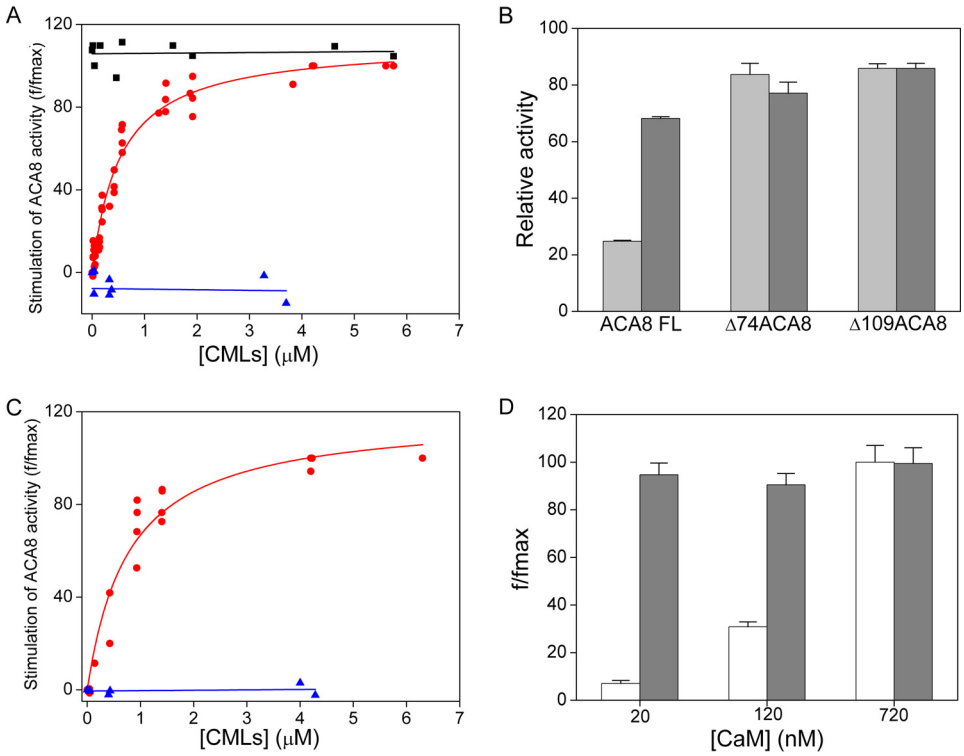

Figure 6. Activation of ACA8 as a function of increasing CML36-C concentrations. Ca^{2+}-ATPase activity of yeast microsomes overexpressing ACA8 (*A*) or of the purified pump (*C*) was measured at the specified CML36-C concentrations in the presence (*squares*) or absence (*circles*) of 1 μM CaM. Activation by CML14 was also tested under the same experimental conditions (*triangles*). Enzyme stimulation (*f*/*f*max) is expressed as the ratio between percent of activation at the indicated CML concentrations (*f*) and maximal activation evaluated at the highest CML concentration tested (*f*max; 180–350% in different biological samples). *B*, basal (*light gray bars*) and CML36-C-stimulated (*dark gray bars*) hydrolytic activity of ACA8 full-length (*FL*), Δ74ACA8, and Δ109ACA8. Ca^{2+}-dependent ATPase activity was assayed in yeast microsomes expressing different versions of ACA8 in the presence of 1.9 μM CML36-C. Activities ± S.E. were normalized, setting as 100 the activity measured in the presence of 3 μM CaM to compensate for different levels in protein expression. CaM-stimulated activity ranged between 70 and 170 nmol P_i min^{-1} mg^{-1} protein in different biological samples. *D*, Ca^{2+}-ATPase activity of purified ACA8 measured at the indicated CaM concentrations with (*gray bars*) or without (*white bars*) 4.2 μM CML36-C. Maximal activation (*f*max) was evaluated at the highest CaM concentration tested.

more abundant in roots and inflorescences (Fig. 7*A* and supplemental Fig. S2*A*). This expression pattern showed a similar trend when either actin (Fig. 7*A*) or a subunit of phosphatase 2A (47) (supplemental Fig. S2*A*) was used as a reference gene for normalization. Our data agree with the *Arabidopsis* microarray expression data available at AtGenExpress Visualization Tool. *ACA8* expression was found in all organs examined, with the highest levels in inflorescences (Fig. 7*B* and supplemental Fig. S2*B*) (48).

Discussion

Given the abundance of CaM/CML in plants, the definition of their properties as Ca^{2+} sensors and the identification of their downstream targets represent an impressive challenge. Herein, we have presented structural and biochemical studies demonstrating that recombinant CML36 from *A. thaliana* displays the typical properties of proteins that function as Ca^{2+} sensors and can stimulate the hydrolytic activity of the *Arabidopsis* ACA8 isoform by specifically binding to the N-terminal regulative domain of ACA8. CML36 possesses the characteristics of regulatory EF-hand Ca^{2+}-binding proteins including, upon Ca^{2+} binding: (i) an increase in α-helical content; (ii) a shift in electrophoretic mobility; (iii) the adoption of a stable tertiary structure; and (iv) the exposure of a hydrophobic pocket that can interact with an ANS probe as a result of the Ca^{2+}-induced conformational changes, which is often a critical process for the function of many Ca^{2+} sensor proteins. In addition, we obtained information on the site-specific Ca^{2+} binding affinities of CML36, which are crucial because Ca^{2+} affinity is often attuned to the physiological role of the Ca^{2+} sensor protein. We found that CML36 possesses two mixed Ca^{2+}/Mg^{2+}-binding sites of high affinity ($K_{dCa} < 0.2$ μM and $K_{dMg} \sim 100$ μM) and two Ca^{2+}-specific sites of low affinity ($\geq$100 μM). The NMR data indicate that CML36 binds the two Mg^{2+} ions to EF-3 and EF-4; therefore, EF-3 and EF-4 represent the Ca^{2+}/Mg^{2+} high-affinity sites, whereas EF-1 and EF-2 are the low-affinity sites. Notably, all four EF-hands of the protein are capable of sensing Ca^{2+} ions. This finding was unexpected, as only three EF-hands were predicted to be functional Ca^{2+}-binding sites by PROSITE-ProRule annotation (49). Indeed, EF-2 (residues 108–127) possesses an arginine residue at position 9 of the loop, where a hydrophilic or negative side chain is usually hydrogen-bonded to a Ca^{2+}-ligand water molecule, and thus it is not predicted to have functional Ca^{2+} binding, although the canonical Ca^{2+}-coordinating groups at positions 1, 3, 5, 7, and 12 are present. It is tempting to attribute this EF-hand to the lowest-affinity site. Further, the reduced affinity of EF-1 could be ascribed to the replacement of a conserved glutamate residue with an aspartate at position 12 (8). Future studies of Ca^{2+}-bound CML36 X-ray structures will be helpful in elucidating the difference in the microenvironment of the EF-hands at the

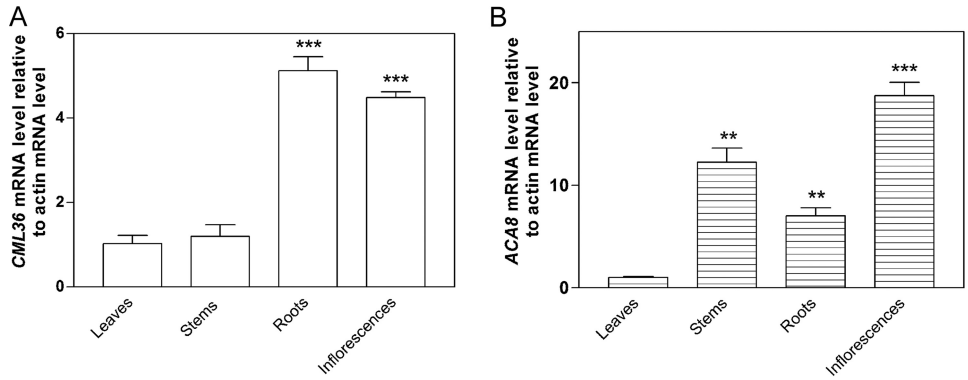

Figure 7. Analysis of *CML36* and *ACA8* expression in *Arabidopsis*. Quantitative RT-PCR of *CML36* (*A*) and *ACA8* (*B*) was performed in various organs of wild-type adult plants. The expression levels were normalized using actin as the endogenous control gene, and the relative expression ratios were calculated using leaves as the calibrator sample. The values reported are means ± S.E. ($n = 3$); Student's *t* test was applied: **, $p < 0.01$, and ***, $p < 0.001$ *versus* leaves.

atomic level, which will facilitate understanding of these site-specific Ca^{2+} affinity properties.

Notably, Mg^{2+} binding to high-affinity EF-3 and EF-4 sites also induces a global conformational change throughout CML36 that results in the stabilization of its tertiary structure. Cation binding to the Ca^{2+}/Mg^{2+} mixed sites seems to control an important structural transition from a molten globule state to a compact globular conformation. Indeed, we found that, similar to other Ca^{2+}-binding proteins (24, 25, 28, 50), apoCML36 likely assumes a molten globule structure and the transition from this molten globule to the compact state clearly occurs when the high-affinity sites are occupied by either Ca^{2+} or Mg^{2+}.

The observed binding constants of Ca^{2+}/Mg^{2+} mixed sites for Mg^{2+} and for Ca^{2+} imply that under resting conditions these two EF-hands are always occupied by a divalent cation, ensuring a folded ion-bound structure of CML36 at any cytoplasmic Ca^{2+} concentration. Next, in response to the rapid increase in intracellular Ca^{2+} concentrations upon a stimulus, the Ca^{2+}-bound state becomes the dominant state of the protein, able to displace Mg^{2+} from these EF-hands.

Beyond the description of the structural and metal-binding properties of CML36, a significant advancement in the knowledge about this protein has been obtained by the identification of ACA8 as a CML36 downstream target. As a strategical isoform of PM-localized Ca^{2+} pumps in the shaping of intracellular Ca^{2+} dynamics (18), ACA8 is the target of regulation by multiple Ca^{2+}-dependent effectors (17, 18, 42). We have provided direct evidence that ACA8 is also able to interact with the Ca^{2+} sensor CML36 *in vitro* and that this interaction results in the activation of its Ca^{2+}-dependent hydrolytic activity with a $K_{0.5}$ value in the submicromolar range. Neither this interaction nor the activation of ACA8 is detectable with other isoforms of CMLs such as CML19 and CML14, suggesting that ACA8 may be specific for CML36. Moreover, native PAGE analysis allowed us to identify the binding site for CML36 at the N-terminal regulative domain of ACA8. The interaction of CML36 with the N terminus of ACA8 is also supported by our observations that the effects of CML36 and CaM on ACA8 activity are not additive and that variants of ACA8 without the N-terminal CaM-binding domains are completely insensitive to CML36. Nevertheless, further investigations will be necessary to precisely localize the CML-binding site within the N-terminal portion.

The capacity of both CaM and CML36 to bind ACA8 raises the question of which mechanisms are capable of avoiding promiscuous interactions in cell-regulatory processes. The choice of the proper signaling pathway involving CML36 or CaM may be related to many modulating factors: (i) the abundance of each protein in a specific microdomain, cellular compartment, tissue and organ; (ii) the time-dependent expression in differentiation and development; (iii) the temporal and spatial features of the Ca^{2+} signal; (iv) the properties of the EF-hand proteins, such as the Ca^{2+} affinity, the number of functional binding sites, and the ability to discriminate between Ca^{2+} and Mg^{2+}; and (v) site-specific phosphorylation. In this scenario, it is worth noting that the predicted affinities of CML36 for Ca^{2+} differ significantly from those observed for mammalian and *Arabidopsis* CaM1 (29, 51); this would influence the ability of these Ca^{2+} sensors to respond to cytosolic Ca^{2+} increases induced by the perception of different stimuli and thus their ability to activate their downstream targets as ACA8. Moreover, the *CML36* and *ACA8* genes are co-expressed mainly in shoot inflorescences. Furthermore, CML36 displays an elongated N terminus, which may represent a targeting sequence. Indeed, a mass spectrometry–based quantitative phosphoproteomics approach identifies CML36 as a protein associated with the PM fraction (37), which might facilitate the interaction with ACA8 *in vivo*.

PM-localized Ca^{2+} pumps are likely to play a key role in returning cytosolic Ca^{2+} to resting concentrations and in modulating the dynamics of a Ca^{2+} signature (2, 5). Analysis of *ACA8* expression, which is up-regulated upon cold stress and abscisic acid treatment, supports its involvement in crucial processes such as response to abiotic stresses and hormonal regulation (48, 52). Furthermore, genetic evidence using KO plant mutants also indicates additional roles for ACA8 in developmental processes and plant immune response (36). Expression of the *CML36* gene also suggests a possible role in organ development for CML36. Interestingly, the *CML36* transcript has been found to be altered in an *Arabidopsis* double mutant lacking both ACA8 and ACA10, another PM-localized Ca^{2+}-ATPase isoform (36). In addition, ACA8 has been recently identified as a prominent *in vivo* regulator of cellular Ca^{2+}

dynamics which crucially functions in the termination of Ca^{2+} signals induced by mechanical wounding and related stimuli (18). In this scenario, CML36 would act in concert with other Ca^{2+} sensors such as CaM (16, 39, 53, 54), CDPK (42), and the CBL-CIPK complexes (18) to regulate ACA8 activity. In addition, other CMLs may be involved in the modulation of ACA8 and other different isoforms of autoinhibited Ca^{2+} pumps, which might contribute to the elaborated/intricate Ca^{2+}-dependent regulatory network for the fine-tuning of intracellular Ca^{2+} homeostasis.

Experimental procedures

Protein production

The coding sequence for CML36 (*At3g10190*) was PCR-amplified using pUNI51-U23411 vector as template obtained from The Arabidopsis Information Resource (TAIR). The following primers were employed: forward, 5′-CATATGCACCAC CACCACCACCACATGAAACTCGCCAAAC-3′; and reverse, 5′-GAATTCTCAACGCTGGAGATCCATCATTCGTGAG-3′. The forward primer carried a NdeI restriction site and a His_6 tag, and the reverse primer contained a stop codon and an EcoRI restriction site. The verified cDNA sequence was then cloned into the corresponding restriction sites of pET21a vector for expression in *Escherichia coli* BL21(DE3) cells. Cells were grown in LB medium at 37 °C to $A_{600\,nm} = 0.6$, and expression of CML36 protein was then induced at 25 °C for 16 h by the addition of 0.4 mM IPTG. To express ^{15}N-labeled CML36 for NMR studies, M9 minimal medium supplemented with $^{15}NH^4Cl$ (1 g liter^{-1}) was employed. The bacterial pellet obtained after low-speed centrifugation of a 1-liter culture was solubilized in 20 mM Tris-HCl, pH 7.5, 150 mM KCl, 10 mM imidazole, and 1 mM DTT lysis buffer containing 0.1 mg ml^{-1} lysozyme, stirred at room temperature for 30 min, and then sonicated on ice. The lysate was centrifuged at 30,000 × *g* for 10 min at 4 °C, and the supernatant was loaded onto a nickel-affinity column pre-equilibrated in 20 mM Tris-HCl, pH 7.5, 150 mM KCl, 1 mM DTT, and 10 mM imidazole buffer. A gradient of imidazole from 10 to 500 mM was applied to the column, and the His-tagged CML36 was eluted around 100 mM imidazole. The fractions containing CML36 were pooled and washed extensively at 4 °C with 20 mM Tris-HCl, pH 7.5, 150 mM KCl, and 1 mM DTT using Vivaspin concentrators (Sartorius, Goettingen, Germany) to remove the imidazole. Protein concentration was determined using the Bio-Rad assay.

cDNA encoding N-terminally truncated CML36 was generated by PCR using the complete cDNA of CML36 as template, a forward primer containing a NdeI site (5′-CATATGCATCAT-CATCATCATCACGAGGTTCCTTCTCCTTATTC-3′) and a reverse primer containing a EcoRI site (5′-GAATTCTT-CAACGCTGGAGATCCATCATTCGTGAG-3′). The resulting DNA fragment was inserted into pET21a using the NdeI/EcoRI sites for directional cloning. The newly generated plasmid was checked by DNA sequencing and used to transform *E. coli* BL21(DE3) cells. The conditions for expression and purification of the deletion mutant were as described for CML36 f.l. The yield was about 6 mg and 100 mg for a 1-liter culture for the full-length protein and the N-terminally truncated variant, respectively. Purified CML36 variants were treated with 2 mM EGTA, washed extensively against decalcified buffer and then against decalcified NH_4HCO_3 buffer, lyophilized, and stored at −80 °C until use. Buffers were decalcified by using Chelex-100 ion-exchange resin (Sigma) according to the manufacturer's instructions. The residual Ca^{2+} concentration was determined using 5,5′-Br2-BAPTA (5,5′-dibromobis-(*o*-aminophenoxy)ethane-*N*,*N*,*N*′,*N*′-tetraacetic acid) as described (55, 56).

AtCaM1 and CML14 were produced as described (43, 57). CML19 was expressed and purified as reported in the supplemental "Methods". The production of recombinant ACA8-N, the N-terminal domain of ACA8 (residues 1–116) was performed as described (54, 58).

The Ca^{2+}-induced mobility shift of CML36-C was performed on a 12.5% Tris-glycine native PAGE and a 15% SDS-PAGE after incubating CML36-C with 5 mM $CaCl_2$ or 5 mM EGTA for 30 min at room temperature.

Nuclear magnetic resonance spectroscopy

NMR spectra were collected on a 600-MHz Bruker Avance III spectrometer (Bruker, Karlsruhe, Germany) equipped with a cryogenic probe. A standard ^1H-^{15}N HSQC pulse sequence was used with pulsed-field gradients for suppression of the solvent signal. ^1H-^{15}N HSQC experiments were collected with a data matrix of 12 ppm (^1H) × 36 ppm (^{15}N), 8 scans, and a 1.2-s relaxation delay.

To achieve partial backbone atom assignment of CML36-C bound to Ca^{2+} or Mg^{2+} ions, standard triple resonance NMR experiments were acquired on ^{15}N,^{13}C-labeled samples (59). The PFG-STE (pulsed-field gradient-stimulated echo) experiments, employing bipolar gradients (60), were conducted and analyzed as described previously (61). DSS (1 mM final concentration) was added to the protein samples and used as an internal standard (62). Delays of 25 and 180 ms between the defocusing and refocusing gradient elements were employed for experiments on DSS and protein samples, respectively. Spectra were acquired with 8000 complex points and 128 transients. The R_h values of the proteins were calculated based on the relationship $R_b^{prot} = (D_{DSS}/D_{prot})\ R_b^{ref}$, where R_b^{ref} is the hydrodynamic radius reported for DSS (3.43 Å) and D_{DSS} and D_{prot} are the diffusion coefficients calculated as described for the DSS and the protein, respectively. The spectra were recorded at 25 °C in 20 mM Tris-HCl, 1 mM DTT, pH 7.5, at a protein concentration of 500 μM in the presence of 5 mM EGTA, 5 mM $MgCl_2$, or 5 mM $CaCl_2$ and analyzed with Topspin3.2 (Bruker, Karlsruhe, Germany).

Size-exclusion chromatography

The hydrodynamic radius of apoCML36-C and Mg^{2+}- and Ca^{2+}-bound CML36-C was estimated by SEC using a Superose 12 column (10/300GL, GE Healthcare) as described previously (43, 63). Each experiment was performed at least in triplicate, and the reported values represent means ± S.E.

Spectroscopic measurements

CD spectra were collected on a Jasco J-710 spectropolarimeter at 25 °C in 20 mM Tris-HCl,150 mM KCl, and 1 mM DTT, pH

7.5, in the presence of 5 mM EGTA, 5 mM $CaCl_2$, or 5 mM $MgCl_2$. Protein concentration was ~90 μM in a cuvette with a path length of 1 cm for near-UV wavelengths, and for far-UV spectra the CML36-C concentration was 10 μM in a cuvette with a 0.1-cm path length. Three spectra, averaged automatically, were recorded for each sample as described (29). The ANS fluorescence spectra were recorded on a Jasco FP8200 spectrofluorometer as described (29).

Isothermal titration calorimetry

ITC experiments were performed on a TA Instruments Nano ITC as described (29, 43). All solutions were degassed prior to the rinsing and loading of both the titration and sample cells. The buffer used was decalcified 20 mM Tris-HCl, 150 mM KCl, pH 7.5. Lyophilized CML36-C was resuspended in decalcified buffer.

For Ca^{2+} titrations into 200 μM apoCML36-C or Mg^{2+}-saturated CML36-C, 4 mM $CaCl_2$ was injected with a 0.3-μl injection to displace air from the syringe followed by 40 × 1.25-μl injections. Mg^{2+}-saturated CML36-C was prepared by incubating apoCML36-C for 15 min at 25 °C with 5 mM $MgCl_2$. For experiments in which Mg^{2+} was injected into the apoCML36-C, a 5 mM $MgCl_2$ stock was added to 170 μM apoCML36 by a 1-μl injection to displace air from the syringe followed by 24 × 2-μl injections.

The heats of dilution, collected by injecting Ca^{2+} or Mg^{2+} into buffer without the protein in the sample cell, were subtracted from the raw integrated heats in the presence of protein. Data were fitted using the best-fitting model for each experiment (sequential, two-site, or one-site model). The reported values represent the mean ± S.E. of at least three independent titrations.

The fitted K_a values were converted to K_d values using the equation,

$$K_d = \frac{1}{K_a} \quad \text{(Eq. 1)}$$

Native PAGE analysis

The formation of the complex following ACA8 binding was analyzed under native conditions as described previously (29). Briefly, CML36 f.l., CML36-C, *Arabidopsis* CaM1, CML14, and CML19 were dissolved at a 10 μM concentration in 100 mM Tris, pH 7.5, 5 mM $CaCl_2$, and 4 M urea and incubated in the presence of an excess of recombinant ACA8-N for 1 h at room temperature. Samples were assayed on a 12.5% continuous gel containing 5 mM $CaCl_2$ and 4 M urea. Urea was added either to the gel and the incubation buffer to prevent any nonspecific interactions.

Yeast strain and isolation of microsomes overexpressing ACA8

Saccharomyces cerevisiae strain K616 (MATα pmr1:: HIS3 pmc1:: TRP1 cnb1::LEU2, ade2, ura3; (44)) was used for ACA8 expression (38). Microsomes from yeast cells expressing full-length ACA8 and ACA8-deleted mutants (40, 46) were prepared as reported previously (38). Protein concentration was determined using the Bio-Rad assay.

ACA8 purification from microsomes

Yeast microsomes were solubilized as reported (45) and incubated (45 mg of microsomes) overnight at 4 °C on 4 ml of CaM-Sepharose 4B gel (GE Healthcare). Purification was performed as described (45). The 1 mM EGTA-eluted fraction, added with stoichiometric $CaCl_2$, was concentrated about 70-fold on Vivaspin ultrafiltration spin columns, with a 30-kDa cutoff (Sartorius, Goettingen, Germany), and immediately used for testing Ca^{2+}-ATPase activity or for overlay analysis. For quantification, 1 μl of the concentrated eluate was loaded onto a precast Tris-Tricine polyacrylamide gel (4–12% linear gradient; Anamed, Darmstadt, Germany) with increasing amounts of β-galactosidase used as the standard. After staining with Coomassie Blue, signal quantification was carried out using AlphaEaseFC software by Alpha-Innotech (MMedical, MI, Italy). ACA8 was purified to virtual homogeneity.

Ca^{2+}-ATPase activity assay

ACA8 activity in yeast microsomes (0.4 mg of protein/ml) and in the EGTA-purified fraction (0.03 mg of protein/ml) was assayed as Ca^{2+}-dependent MgITP or MgATP hydrolysis, respectively, as described (40, 42). Free Ca^{2+} concentration was buffered at 10 μM with 1 mM EGTA. Bovine testes CaM (Sigma-Aldrich) and *A. thaliana* purified Ca^{2+}-bound CML36 or CML14 were added at the specified concentrations. Assays were performed by preincubating CMLs with microsomes or ACA8-purified protein in assay buffer for 20 min at 25 °C before starting the reaction by the addition of nucleotide substrates. Samples were then incubated at 25 °C for 60 min. MgITP or MgATP hydrolysis measured in the presence of 1 mM EGTA without added Ca^{2+} was subtracted from the reported data. Assays were performed at least four times, with three replicates for each condition, using three independent biological samples and at least two different CML36 preparations. The standard error did not exceed 5% of the mean. Data analysis and curve fitting were performed using SigmaPlot software. $K_{0.5}$ for CML36 (±S.E.) was estimated using nonlinear regression. Student's t test was conducted to assess potential differences between $K_{0.5}$ estimated from data obtained using yeast microsomes and purified ACA8 ($p = 0.1173$).

Overlay assay

Different amounts of purified Ca^{2+}-bound CML36 (0.6, 0.12, and 0.03 nmol), 0.6 nmol of purified Ca^{2+}-bound CML14, 0.6 nmol of lysozyme (Sigma-Aldrich), and 0.03 nmol of bovine testes CaM (Sigma-Aldrich) were spotted onto 0.2-μm nitrocellulose. Proteins were first cross-linked to the membrane by incubating them for 45 min at room temperature in 0.2% (v/v) glutaraldehyde freshly prepared in KP buffer (25 mM KH_2/K_2HPO_4 buffer, pH 7). The membrane was incubated thereafter for 16 h in blocking solution (3% (w/v) BSA, 0.15 M NaCl, 2 mM $MgSO_4$, 0.2% (v/v) polyoxyethylene (20) sorbitan monolaurate, and 20 mM Tris-HCl, pH 7.4). After washing, the overlay was conducted by incubating the membrane for 2 h at room temperature in blocking solution with 1.5 μM purified ACA8 or, in parallel as a negative control, in the same solution without ACA8. Following a fast wash in blocking solution, an additional 45-min cross-linking step was carried out. Immunodetection

with an antiserum against the sequence ^{268}EISIYDIVVGDVIPLNIGNQVPADGVLISGHSLALDESSMTGESKIVNKDANKDPFLMSGCKVADGNGSMLVTGVGVNTEW^{348} of ACA8 was performed as described (58).

Plant material, growth conditions, and gene expression analysis by quantitative reverse transcription-PCR

To evaluate *CML36* gene expression in various adult organs, *A. thaliana* ecotype Columbia (Col-0) seeds were sown on soil in a greenhouse under a 16-h light/8-h dark photoperiod at 24 °C and 20 °C, respectively; the plants were grown to maturity. The isolation of total RNA was performed using the RNeasy mini kit (Qiagen, Hilden, Germany) from 100 mg of frozen organs, and then the RNA samples were treated with RQ1 RNase-free DNase (Promega, Madison, WI). cDNA synthesis was obtained with oligo-(dT) primer and carried out using the GoScript reverse transcription system (Promega). SYBR Green qPCR Supermix-UDG (Invitrogen) was used to amplify cDNA on the StepOnePlus™ real-time PCR system (Applied Biosystems, Foster City, CA). Quantitative RT-PCR was performed using the following cycling conditions: 2 min at 50 °C, 2 min at 95 °C, 40 cycles of 95 °C for 30 s, 59 °C for 30 s, 72 °C for 30 s, and finally 72 °C for 3 min. The actin gene was used as an endogenous control and to normalize all quantifications. Three cDNA samples obtained from three independent RNA extractions were examined. Relative quantitation of transcript levels was performed as reported (64). The following forward (F) and reverse (R) primers were employed: for *CML36* (*At3g10190*), F, 5′-CATCTTCCGGCCAAGACTGT-3′, and R, 5′-ACCTCCGGGAGAATGCTAGT-3′; for *ACA8* (*At5g57110*), F, 5′-AAGTCCTTACCGTAGCGGTTACAA-3′ and R, 5′-ATTGAATAGGCAAGGGTTAAAGTAACA-3′ (48). Two internal reference genes, an actin gene (*At3g18780*) and a subunit of phosphatase 2A (*PP2A At1g13320*), were used for data normalization (47, 65). The following primers were employed: for actin, F, 5′-TGTTCTCTCCTTGTACGCCAGT-3′, and R, 5′-CAGCAAGGTCAAGACGGAGGA-3′; and for *PP2A*, F 5′-TAACGTGGCCAAAATGATGC-3′, and R, 5′-GTTCTCCACAACCGCTTGGT-3′ (47).

Author contributions—A. A. and P. D. conceived the study. A. A. coordinated the study and wrote the paper. A. A., R. V., and V. L. V. produced the recombinant proteins, designed, performed, and analyzed the structural, metal-binding, and native PAGE experiments. M. C. B. and L. L. carried out overlay and activity assays. M. C. B. participated in drafting the article and revising it critically. M. D. performed the NMR experiments. B. M. carried out gene expression analysis. All authors analyzed the results and approved the final version of the manuscript.

Acknowledgments—We are grateful to Prof. M. I. De Michelis and Prof. A. Costa (University of Milano) for fruitful discussions and critical reading of the manuscript. We thank Prof. M. Bertoldi (University of Verona) for help with the CD experiments. We also thank the "Centro Piattaforme Tecnologiche" of the University of Verona for providing access to the NMR spectrometer and nanoITC calorimeter.

References

1. Sanders, D., Pelloux, J., Brownlee, C., and Harper, J. F. (2002) Calcium at the crossroads of signaling. *Plant Cell* **14,** S401–S417
2. Dodd, A. N., Kudla, J., and Sanders, D. (2010) The language of calcium signaling. *Annu. Rev. Plant Biol.* **61,** 593–620
3. Kudla, J., Batistic, O., and Hashimoto, K. (2010) Calcium signals: The lead currency of plant information processing. *Plant Cell* **22,** 541–563
4. Steinhorst, L., and Kudla, J. (2013) Calcium and reactive oxygen species rule the waves of signaling. *Plant Physiol.* **163,** 471–485
5. McAinsh, M. R., and Pittman, J. K. (2009) Shaping the calcium signature. *New Phytol.* **181,** 275–294
6. Webb, A. A. R., McAinsh, M. R., Taylor, J. E., and Hetherington, A. M. (1996) Calcium ions as intracellular second messengers in higher plants, in *Advances in Botanical Research* (Callow, J. A., ed) pp 45–96, Academic Press, Orlando, FL
7. Luan, S., Kudla, J., Rodriguez-Concepcion, M., Yalovsky, S., and Gruissem, W. (2002) Calmodulins and calcineurin B-like proteins: Calcium sensors for specific signal response coupling in plants. *Plant Cell* **14,** Suppl., S389–S400
8. Gifford, J. L., Walsh, M. P., and Vogel, H. J. (2007) Structures and metal-ion-binding properties of the Ca2+-binding helix-loop-helix EF-hand motifs. *Biochem. J.* **405,** 199–221
9. Permyakov, E. A., and Kretsinger, R. H. (2010) Index, in *Calcium Binding Proteins*, pp. 567–573, John Wiley & Sons, Inc., New York
10. McCormack, E., and Braam, J. (2003) Calmodulins and related potential calcium sensors of *Arabidopsis*. *New Phytol.* **159,** 585–598
11. McCormack, E., Tsai, Y. C., and Braam, J. (2005) Handling calcium signaling: *Arabidopsis* CaMs and CMLs. *Trends Plant Sci.* **10,** 383–389
12. Bender, K. W., and Snedden, W. A. (2013) Calmodulin-related proteins step out from the shadow of their namesake. *Plant Physiol.* **163,** 486–495
13. Perochon, A., Aldon, D., Galaud, J. P., and Ranty, B. (2011) Calmodulin and calmodulin-like proteins in plant calcium signaling. *Biochimie* **93,** 2048–2053
14. Zeng, H., Xu, L., Singh, A., Wang, H., Du, L., and Poovaiah, B. W. (2015) Involvement of calmodulin and calmodulin-like proteins in plant responses to abiotic stresses. *Front. Plant Sci.* **6,** 600
15. Ranty, B., Aldon, D., Cotelle, V., Galaud, J. P., Thuleau, P., and Mazars, C. (2016) Calcium sensors as key hubs in plant responses to biotic and abiotic stresses. *Front. Plant Sci.* **7,** 327
16. Bonza, M. C., Morandini, P., Luoni, L., Geisler, M., Palmgren, M. G., and De Michelis, M. I. (2000) At-ACA8 encodes a plasma membrane-localized calcium-ATPase of *Arabidopsis* with a calmodulin-binding domain at the N terminus. *Plant Physiol.* **123,** 1495–1506
17. Bonza, M. C., and De Michelis, M. I. (2011) The plant Ca2+ -ATPase repertoire: Biochemical features and physiological functions. *Plant Biol. (Stuttg.)* **13,** 421–430
18. Costa, A., Luoni, L., Marrano, C. A., Hashimoto, K., Koster, P., Giacometti, S., De Michelis, M. I., Kudla, J., and Bonza, M. C. (2017) Ca2+-dependent phosphoregulation of the plasma membrane Ca2+-ATPase ACA8 modulates stimulus-induced calcium signatures. *J. Exp. Bot.* 10.1093/jxb/erx162
19. Kozlowski, L. P., and Bujnicki, J. M. (2012) MetaDisorder: A meta-server for the prediction of intrinsic disorder in proteins. *BMC Bioinformatics* **13,** 111
20. Waters, B. M. (2011) Moving magnesium in plant cells. *New Phytol.* **190,** 510–513
21. Maathuis, F. J. (2009) Physiological functions of mineral macronutrients. *Curr. Opin. Plant Biol.* **12,** 250–258
22. Grabarek, Z. (2011) Insights into modulation of calcium signaling by magnesium in calmodulin, troponin C and related EF-hand proteins. *Biochim. Biophys. Acta* **1813,** 913–921
23. Ames, J. B., Dizhoor, A. M., Ikura, M., Palczewski, K., and Stryer, L. (1999) Three-dimensional structure of guanylyl cyclase-activating protein-2, a calcium-sensitive modulator of photoreceptor guanylyl cyclases. *J. Biol. Chem.* **274,** 19329–19337
24. Ames, J. B., Hendricks, K. B., Strahl, T., Huttner, I. G., Hamasaki, N., and Thorner, J. (2000) Structure and calcium-binding properties of Frq1, a

novel calcium sensor in the yeast *Saccharomyces cerevisiae*. *Biochemistry* **39,** 12149–12161
25. Yamniuk, A. P., Nguyen, L. T., Hoang, T. T., and Vogel, H. J. (2004) Metal ion binding properties and conformational states of calcium- and integrin-binding protein. *Biochemistry* **43,** 2558–2568
26. Sorensen, B. R., and Shea, M. A. (1996) Calcium binding decreases the stokes radius of calmodulin and mutants R74A, R90A, and R90G. *Biophys. J.* **71,** 3407–3420
27. Sorensen, B. R., Eppel, J. T., and Shea, M. A. (2001) Paramecium calmodulin mutants defective in ion channel regulation associate with melittin in the absence of calcium but require it for tertiary collapse. *Biochemistry* **40,** 896–903
28. Osawa, M., Dace, A., Tong, K. I., Valiveti, A., Ikura, M., and Ames, J. B. (2005) Mg2+ and Ca2+ differentially regulate DNA binding and dimerization of DREAM. *J. Biol. Chem.* **280,** 18008–18014
29. Astegno, A., La Verde, V., Marino, V., Dell'Orco, D., and Dominici, P. (2016) Biochemical and biophysical characterization of a plant calmodulin: Role of the N- and C-lobes in calcium binding, conformational change, and target interaction. *Biochim. Biophys. Acta* **1864,** 297–307
30. Eldik, L. J., Grossman, A. R., Iverson, D. B., and Watterson, D. M. (1980) Isolation and characterization of calmodulin from spinach leaves and *in vitro* translation mixtures. *Proc. Natl. Acad. Sci. U.S.A.* **77,** 1912–1916
31. Burgess, W. H., Jemiolo, D. K., and Kretsinger, R. H. (1980) Interaction of calcium and calmodulin in the presence of sodium dodecyl sulfate. *Biochim. Biophys. Acta* **623,** 257–270
32. Garrigos, M., Deschamps, S., Viel, A., Lund, S., Champeil, P., Møller, J. V., and le Maire, M. (1991) Detection of Ca(2+)-binding proteins by electrophoretic migration in the presence of Ca2+ combined with 45Ca2+ overlay of protein blots. *Anal. Biochem.* **194,** 82–88
33. Gifford, J. L., Jamshidiha, M., Mo, J., Ishida, H., and Vogel, H. J. (2013) Comparing the calcium binding abilities of two soybean calmodulins: Towards understanding the divergent nature of plant calmodulins. *Plant Cell* **25,** 4512–4524
34. Dobney, S., Chiasson, D., Lam, P., Smith, S. P., and Snedden, W. A. (2009) The calmodulin-related calcium sensor CML42 plays a role in trichome branching. *J. Biol. Chem.* **284,** 31647–31657
35. Szklarczyk, D., Franceschini, A., Kuhn, M., Simonovic, M., Roth, A., Minguez, P., Doerks, T., Stark, M., Muller, J., Bork, P., Jensen, L. J., and von Mering, C. (2011) The STRING database in 2011: Functional interaction networks of proteins, globally integrated and scored. *Nucleic Acids Res.* **39,** D561–D568
36. Frei dit Frey, N., Mbengue, M., Kwaaitaal, M., Nitsch, L., Altenbach, D., Häweker, H., Lozano-Duran, R., Njo, M. F., Beeckman, T., Huettel, B., Borst, J. W., Panstruga, R., and Robatzek, S. (2012) Plasma membrane calcium ATPases are important components of receptor-mediated signaling in plant immune responses and development. *Plant Physiol.* **159,** 798–809
37. Benschop, J. J., Mohammed, S., O'Flaherty, M., Heck, A. J., Slijper, M., and Menke, F. L. (2007) Quantitative phosphoproteomics of early elicitor signaling in *Arabidopsis*. *Mol. Cell. Proteomics* **6,** 1198–1214
38. Bonza, M. C., Luoni, L., and De Michelis, M. I. (2004) Functional expression in yeast of an N-deleted form of At-ACA8, a plasma membrane Ca(2+)-ATPase of *Arabidopsis thaliana*, and characterization of a hyperactive mutant. *Planta* **218,** 814–823
39. Luoni, L., Bonza, M. C., and De Michelis, M. I. (2006) Calmodulin/Ca2+-ATPase interaction at the *Arabidopsis thaliana* plasma membrane is dependent on calmodulin isoform showing isoform-specific Ca2+ dependencies. *Physiol. Plant.* **126,** 175–186
40. Bonza, M. C., and Luoni, L. (2010) Plant and animal type 2B Ca2+-ATPases: Evidence for a common auto-inhibitory mechanism. *FEBS Lett.* **584,** 4783–4788
41. Meneghelli, S., Fusca, T., Luoni, L., and De Michelis, M. I. (2008) Dual mechanism of activation of plant plasma membrane Ca2+-ATPase by acidic phospholipids: Evidence for a phospholipid binding site which overlaps the calmodulin-binding site. *Mol. Membr. Biol.* **25,** 539–546
42. Giacometti, S., Marrano, C. A., Bonza, M. C., Luoni, L., Limonta, M., and De Michelis, M. I. (2012) Phosphorylation of serine residues in the N terminus modulates the activity of ACA8, a plasma membrane Ca2+-ATPase of *Arabidopsis thaliana*. *J. Exp. Bot.* **63,** 1215–1224
43. Vallone, R., La Verde, V., D'Onofrio, M., Giorgetti, A., Dominici, P., and Astegno, A. (2016) Metal binding affinity and structural properties of calmodulin-like protein 14 from *Arabidopsis thaliana*. *Protein Sci.* **25,** 1461–1471
44. Cunningham, K. W., and Fink, G. R. (1994) Calcineurin-dependent growth control in *Saccharomyces cerevisiae* mutants lacking PMC1, a homolog of plasma membrane Ca2+ ATPases. *J. Cell Biol.* **124,** 351–363
45. Fusca, T., Bonza, M. C., Luoni, L., Meneghelli, S., Marrano, C. A., and De Michelis, M. I. (2009) Single point mutations in the small cytoplasmic loop of ACA8, a plasma membrane Ca2+-ATPase of *Arabidopsis thaliana*, generate partially deregulated pumps. *J. Biol. Chem.* **284,** 30881–30888
46. Calì, T., Frizzarin, M., Luoni, L., Zonta, F., Pantano, S., Cruz, C., Bonza, M. C., Bertipaglia, I., Ruzzene, M., De Michelis, M. I., Damiano, N., Marin, O., Zanni, G., Zanotti, G., Brini, M., *et al.* (2017) The ataxia-related G1107D mutation of the plasma membrane Ca2+ ATPase isoform 3 affects its interplay with calmodulin and the autoinhibition process. *Biochim. Biophys. Acta* **1863,** 165–173
47. Czechowski, T., Stitt, M., Altmann, T., Udvardi, M. K., and Scheible, W. R. (2005) Genome-wide identification and testing of superior reference genes for transcript normalization in *Arabidopsis*. *Plant Physiol.* **139,** 5–17
48. Cerana, M., Bonza, M. C., Harris, R., Sanders, D., and De Michelis, M. I. (2006) Abscisic acid stimulates the expression of two isoforms of plasma membrane Ca2+-ATPase in *Arabidopsis thaliana* seedlings. *Plant Biol. (Stuttg.)* **8,** 572–578
49. de Castro, E., Sigrist, C. J., Gattiker, A., Bulliard, V., Langendijk-Genevaux, P. S., Gasteiger, E., Bairoch, A., and Hulo, N. (2006) ScanProsite: Detection of PROSITE signature matches and ProRule-associated functional and structural residues in proteins. *Nucleic Acids Res.* **34,** W362–W365
50. Wingard, J. N., Chan, J., Bosanac, I., Haeseleer, F., Palczewski, K., Ikura, M., and Ames, J. B. (2005) Structural analysis of Mg2+ and Ca2+ binding to CaBP1, a neuron-specific regulator of calcium channels. *J. Biol. Chem.* **280,** 37461–37470
51. Gilli, R., Lafitte, D., Lopez, C., Kilhoffer, M., Makarov, A., Briand, C., and Haiech, J. (1998) Thermodynamic analysis of calcium and magnesium binding to calmodulin. *Biochemistry* **37,** 5450–5456
52. Schiøtt, M., and Palmgren, M. G. (2005) Two plant Ca2+ pumps expressed in stomatal guard cells show opposite expression patterns during cold stress. *Physiol. Plant.* **124,** 278–283
53. Tidow, H., Poulsen, L. R., Andreeva, A., Knudsen, M., Hein, K. L., Wiuf, C., Palmgren, M. G., and Nissen, P. (2012) A bimodular mechanism of calcium control in eukaryotes. *Nature* **491,** 468–472
54. Baekgaard, L., Luoni, L., De Michelis, M. I., and Palmgren, M. G. (2006) The plant plasma membrane Ca2+ pump ACA8 contains overlapping as well as physically separated autoinhibitory and calmodulin-binding domains. *J. Biol. Chem.* **281,** 1058–1065
55. Astegno, A., Maresi, E., Marino, V., Dominici, P., Pedroni, M., Piccinelli, F., and Dell'Orco, D. (2014) Structural plasticity of calmodulin on the surface of CaF2 nanoparticles preserves its biological function. *Nanoscale* **6,** 15037–15047
56. Marino, V., Astegno, A., Pedroni, M., Piccinelli, F., and Dell'Orco, D. (2014) Nanodevice-induced conformational and functional changes in a prototypical calcium sensor protein. *Nanoscale* **6,** 412–423
57. Gut, H., Dominici, P., Pilati, S., Astegno, A., Petoukhov, M. V., Svergun, D. I., Grütter, M. G., and Capitani, G. (2009) A common structural basis for pH- and calmodulin-mediated regulation in plant glutamate decarboxylase. *J. Mol. Biol.* **392,** 334–351
58. Luoni, L., Meneghelli, S., Bonza, M. C., and DeMichelis, M. I. (2004) Autoinhibition of *Arabidopsis thaliana* plasma membrane Ca2+-ATPase involves an interaction of the N terminus with the small cytoplasmic loop. *FEBS Lett.* **574,** 20–24
59. Favretto, F., Santambrogio, C., D'Onofrio, M., Molinari, H., Grandori, R., and Assfalg, M. (2015) Bile salt recognition by human liver fatty acid binding protein. *FEBS J.* **282,** 1271–1288

60. Merrill, M. R. (1993) NMR diffusion measurements using a composite gradient PGSE sequence. *J. Magn. Reson. A* **103,** 223–225
61. Eliseo, T., Ragona, L., Catalano, M., Assfalg, M., Paci, M., Zetta, L., Molinari, H., and Cicero, D. O. (2007) Structural and dynamic determinants of ligand binding in the ternary complex of chicken liver bile acid binding protein with two bile salts revealed by NMR. *Biochemistry* **46,** 12557–12567
62. Wilkins, D. K., Grimshaw, S. B., Receveur, V., Dobson, C. M., Jones, J. A., and Smith, L. J. (1999) Hydrodynamic radii of native and denatured proteins measured by pulse field gradient NMR techniques. *Biochemistry* **38,** 16424–16431
63. Astegno, A., Capitani, G., and Dominici, P. (2015) Functional roles of the hexamer organization of plant glutamate decarboxylase. *Biochim. Biophys. Acta* **1854,** 1229–1237
64. Livak, K. J., and Schmittgen, T. D. (2001) Analysis of relative gene expression data using real-time quantitative PCR and the 2(-ΔΔC(T)) method. *Methods* **25,** 402–408
65. Gutierrez, L., Mauriat, M., Guénin, S., Pelloux, J., Lefebvre, J. F., Louvet, R., Rusterucci, C., Moritz, T., Guerineau, F., Bellini, C., and Van Wuytswinkel, O. (2008) The lack of a systematic validation of reference genes: A serious pitfall undervalued in reverse transcription-polymerase chain reaction (RT-PCR) analysis in plants. *Plant Biotechnol. J.* **6,** 609–618